Communication-less Management Strategy for Electric Vehicle Charging in Droop-controlled Islanded Microgrids

Abdullah Azhar Al-Obaidi, Mohammed Zaki El-Sharafy, Hany E. Z. Farag, Saifullah Shafiq, and Ali Al-Awami

***Abstract*—Adopting high penetration levels of electric vehicles (EVs) necessitates the implementation of appropriate charging management systems to mitigate their negative impacts on power distribution networks. Currently, most of the proposed EV charging management techniques rely on the availability of high-bandwidth communication links. Such techniques are far from realization due to ① the lack of utility-grade communication systems in many cases such as secondary (low-voltage) power distribution systems to which EVs are connected, rural areas, remote communities, and islands, and ② existing fears and concerns about the data privacy of EV users and cyber-physical security. For these cases, appropriate local control schemes are needed to ensure the adequate management of EV charging without violating the grid operation requirements. Accordingly, this paper introduces a new communication-less management strategy for EV charging in droop-controlled islanded microgrids. The proposed strategy is autonomous, as it is based on the measurement of system frequency and local bus voltages. The proposed strategy implements a social charging fairness policy during periods when the microgrid distributed generators (DGs) are in short supply by allocating more system capacity to the EVs with less charging in the past. Furthermore, a novel communication-less EV load shedding scheme is incorporated into the management strategy to provide relief to the microgrid during events of severe undervoltage or underfrequency occurrences due to factors such as high loading or DG outages. Numerical simulations demonstrate the superiority of the proposed strategy over the state-of-the-art controllers in modulating the EV charging demand to counteract microgrid instability.**

***Index Terms*—Charging, battery management, communication-less control, droop control, electric vehicle, islanded microgrid.**

I. Introduction

THE rapid growth of electric vehicle (EV) deployment can significantly increase the charging load, which could lead to negative impacts on the existing infrastructure of power distribution systems [1]. This includes congestion of over-aged assets, increase in power losses, and violation of the system frequency/voltage [2]. In order to address these challenges, researchers have developed both centralized and distributed energy management techniques that regulate EV charging and utilize surplus energy in EV batteries to provide ancillary support to the power grid. On one hand, centralized energy management techniques depend on a single operator/aggregator that coordinates and communicates the charging schedules for individual EVs. On the other hand, the distributed energy management techniques divide the charging scheduling problem into a set of subproblems that are solved by multiple aggregators and/or EVs [3], [4]. Nevertheless, centralized energy management techniques are prone to a single point of failure as well as data privacy and security issues [5]. Furthermore, both centralized and distributed energy management techniques require utility-grade communication links to be connected with individual EV chargers in order to communicate with the grid operator and/or other EVs to coordinate set points of the charger [6]. Such a communication network is typically not available, especially at the secondary distribution level, and thus it requires a costly infrastructure upgrade [7].

In contrast to centralized and distributed energy management techniques, autonomous EV charging techniques can regulate the EV load without the need for a communication network [8]. The basic concept of autonomous charging is to utilize local system measurements at the point of charger connection with the grid to decide the charging level that does not disrupt the grid stability [9]. These techniques help facilitate the adoption of EVs for many power distribution systems that have limited or no communication infrastructure and reduce the computational burden on system operators.

There have been numerous studies in the literature that have proposed autonomous EV charging control schemes. A charging technique based on duty cycles and EV departure time is proposed in [10]. The departure time input by the us-

Manuscript received: April 28, 2023; revised: September 1, 2023; accepted: December 17, 2023. Date of CrossCheck: December 17, 2023. Date of online publication: January 16, 2024.

This work was supported by the Natural Sciences and Engineering Research Council (NSERC) of Canada and Early Researcher Award, Ontario Government, Canada.

A. A. Al-Obaidi (corresponding author) and M. Z. El-Sharafy are with the Independent Electricity System Operator (IESO), Mississauga, Canada (e-mail: a89@yorku.ca; eng.mzaki@hotmail.com).

H. E. Z. Farag is with the Department of Electrical Engineering and Computer Science, York University, Toronto, Canada (e-mail: hefarag@yorku.ca).

S. Shafiq is with the University of Queensland, StLucia QLD 4067, Australia (e-mail: sshafiq@pmu.edu.sa).

A. Al-Awami is with the Department of Electrical Engineering, King Fahd University of Petroleum & Minerals, Dhahran, Saudi Arabia (e-mail: aliawami@kfupm.edu.sa).

DOI: 10.35833/MPCE.2023.000234

er is used to calculate a unique duty cycle that switches on and off the charger at a different rate from other chargers in the system to prevent simultaneous power consumption. Reference [11] also proposes to ① use the user departure time in order to decide whether to charge EV once it is plugged in or ② delay it to avoid peak load time. The methods introduced in [10] and [11] assume that EV users will input their departure time accurately. Nevertheless, this assumption is not always valid and users can "game" these methods by inputting false early departure time to charge their EVs faster. Reference [12] presents an autonomous algorithm based on historical records of system conditions at the EV charger point. This algorithm is not reliable because it does not account for future changes in the system configuration and loading.

Several studies have considered the use of measured voltage at the point of common coupling (PCC) as a direct input to control the EV charging load. For example, [13] introduces a voltage-based EV charging controller that adjusts the charging load through a voltage-droop function. Reference [14] utilizes an autonomous voltage-based EV charging controller and explores its interaction with distributed generators (DGs) in a grid-connected system. Reference [15] proposes a non-linear voltage-based autonomous controller with an exponential function that compares the PCC voltage with a reference voltage to decide the charging rate. A fuzzy-based charging scheme that is sensitive to voltage levels at the PCC is proposed in [16]. Other studies have investigated the control of EV charging based on the system frequency. In this regard, the operation of islanded microgrids (IMGs) is more constrained than grid-connected systems, where the low short-circuit capacity of IMGs could result in frequency deviations as a result of any configuration change [17]. Further, droop-controlled IMGs require the droop of frequency and voltage in order to achieve active and reactive power-sharing. Therefore, it is important to consider the changes in the system frequency in autonomous EV charging control logic in IMGs. A frequency-based controller is introduced in [18], where EV charging load is controlled based on the frequency deviation of the microgrid. Similarly, [19] proposes to use the system frequency to regulate the EV charging load, while the bus voltage is used to control the level of reactive power support of EV to the grid.

Nevertheless, existing research works in this area have the following shortcomings and gaps. First, the communication-less controllers proposed in the literature are very conservative, causing unnecessarily slow charging without fully utilizing the capacity of the microgrid. In this regard, the frequency- and voltage-based controllers proposed in previous studies reduce the EV charging speed even when the system frequency and the bus voltages are above their respective nominal values.

Second, the charging control logic implemented in previous studies can result in unfair allocation of microgrid capacity among EVs. In this context, social charging fairness is defined as the equal share of limited microgrid capacity among EVs when power resources are in short supply [20]. Multiple solutions have been proposed to solve the issue of charging fairness in communication-based EV energy management techniques [21]-[24]. In regards to communication-less techniques, the controller proposed in [18] considers an equal charging rate for EVs in the system. Further, [25] investigates the use of voltage sensitivity to achieve charging fairness among EVs in the system. However, both of the controllers in [18] and [25] allocate power system capacity among EVs based on "memory-less fairness", which is allocating resources fairly at the present moment without consideration of the historical allocations [26]. A memory-less fairness policy equates the EVs that are being charged for hours and the EVs that are just plugged into the system, which does not achieve charging fairness.

Third, the frequency- and voltage-based controllers in [13]-[19] are set to regulate the EV charging load down to the minimum acceptable charging rate and then switch off the charger when the system frequencies and/or bus voltages go below their respective acceptable limits. This creates a discontinuity in controllers that could lead to charging load oscillations around the cut-off point. In this regard, the EV chargers are switched off due to violation of the system operation conditions, i.e., system frequencies and/or bus voltages, and as a result, the system frequencies and/or bus voltages rebound, which cause the chargers to activate again and so forth.

To fill these gaps, this paper aims to develop a communication-less management strategy for EV charging in droop-controlled IMGs via an adaptive Sigmoid-based controller. The strategy considers social charging fairness during periods when the microgrid capacity is limited. The key contributions of this paper are as follows.

1) An adaptive Sigmoid-based controller that manages the charging rate based on the system frequencies and bus voltages is proposed. Compared with previous research works, the proposed controller provides more flexibility and better utilization of the power system capacity in EV charging without jeopardizing stability.

2) A social charging fairness system that assigns priority levels to EVs based on their past charging power allocation is developed. The priority level for each EV is autonomously lowered as its charging allocation in the historical time horizon increases. The priority level is utilized to adjust the Sigmoid-based controller to provide more system capacity to the EVs with higher priority levels.

3) The cut-off point in the controllers proposed in the previous research works has been replaced by a novel communication-less EV load shedding scheme that gets triggered when an under-voltage or under-frequency event occurs in the IMG when the generation does not meet the required demand. The proposed shedding scheme is coordinated with the priority level of EVs to ensure fair EV shedding.

4) A system violation index (SVI) is proposed to quantify the effectiveness of the proposed strategy in reducing violations of system operation constraints that result from EV charging.

Without loss of generality, the following assumptions are made during the development of this paper.

1) Similar to the research works in [14]-[19], it is as-

sumed that the proposed strategy is programmed into all EV smart chargers connected to the microgrid, and cannot be modified by EV users. It is acknowledged that different charging infrastructure providers, EV manufacturers, and even individual EV users may have their own charging strategies or proprietary algorithms. This could be addressed by a gradual integration plan that involves pilot studies, incentives for charger operators, and a transition period to allow for updates and adjustments.

2) All chargers follow the constant current/constant voltage (CC/CV) charging profile, which is widely used in charging EV lithium-ion batteries [27]. While the charging profile simplifies the charging control, it might not cover all possible charging scenarios such as fast-charging stations or newer battery chemistries that need different charging protocols. Future work could involve adapting the proposed strategy to accommodate various charging profiles and technologies.

3) Compared with other residential loads, EVs have a greater degree of flexibility due to the energy stored in their batteries. As a result, during periods when the microgrid is not operating normally, the normal load is prioritized while EV charging load is reduced or interrupted before any other loads. Supplemental approaches can be developed to consider the preferences of EV owners while ensuring the overall stability and resilience of the microgrid. This could involve dynamic pricing mechanisms, or predictive modeling that can enable more user-centered charging control, ensuring that the needs of EV owners are aligned with the microgrid stability and resilience goals.

II. Proposed Communication-less Management Strategy for EV Charging

This section describes the proposed communication-less management strategy for EV charging. The proposed strategy is applied locally by each EV charger in the system without any communication with the system operator or other EV chargers. The block diagram of the proposed strategy is shown in Fig. 1. The proposed strategy receives inputs that are ① local system measurements (i.e., bus voltages and system frequencies) taken at PCC, and ② battery state of charge (SoC) of EV. The proposed strategy calculates the battery SoC increase for each EV once it starts charging. An EV priority system then assigns a priority level to the EV based on how much SoC it gains in the past hours. The priority level of the EV will affect the logic of a Sigmoid-based controller that is responsible for regulating EV charging based on changes in the system frequencies and bus voltages. In this regard, a lower priority level for an EV indicates that a decrease in frequency or voltage will result in a higher reduction of charging speed in comparison to higher priority EVs. Moreover, in situations where the system frequencies or bus voltages go below their respective lower limits despite the reduction of EV charging current to the minimum by Sigmoid-based controller, the proposed strategy could deactivate the EV charger through its shedding scheme to maintain IMG. The proposed strategy is explained in details in the following subsections.

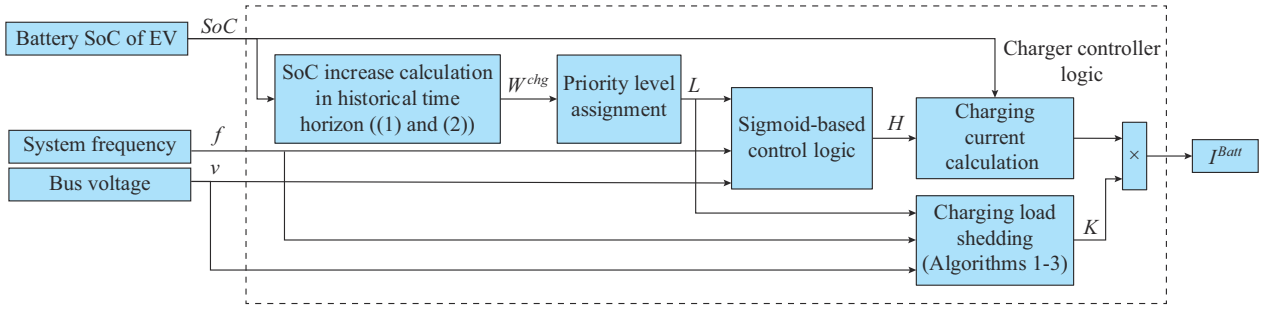

Fig. 1. Proposed strategy for EV charging.

A. EV Priority System

The proposed strategy continuously logs the charging process and calculates the SoC increase of the EV battery in the past time horizon to determine the priority level assigned to the EV. Let D be the set of historical time steps and d be the length of historical time horizon considered with $D=\{t-1, t-2, ..., t-d\}$. This means that if d equals 4 hours for example, the smart charger will continuously calculate the total SoC increase in the last four hours. Parameter d is programmed into all EV smart chargers and can be decided by the IMG operator depending on system requirements. In this regard, a higher SoC increase during the historical time horizon leads to a lower priority assignment in comparison to the EVs with less past charging. The priority level affects the degree to which the EV charging rate is reduced when the system frequencies and/or bus voltages are below their nominal values. In this regard, the choice of the parameter d is guided by several factors that need to be considered. One primary factor is the desired level of responsiveness of the charging control strategy. A shorter d allows for more immediate adjustments to priority levels based on recent charging behavior, whereas a longer d captures a broader charging history, providing a more gradual response. Let t be the time step at which various calculations are performed, where t is used as an index to represent different moments in time during the charging process. The SoC increase of the j^{th} EV at each time step t $SoC_{t,j}$ is estimated by integrating the charging current and adding it to the previous state as [11]:

$$SoC_{t,j} = SoC_{t-1,j} + \frac{1}{C_{Batt}} \int_{t-1}^{t} I_{t,j}^{Batt} \mathrm{d}t \tag{1}$$

where C_{Batt} is the rated capacity of the battery for the j^{th} EV; and $I_{t,j}^{Batt}$ is the charger current of the j^{th} EV at time step t. The total SoC increase $W_{t,j}^{chg}$ during the historical time horizon for the j^{th} EV is calculated as:

$$W_{t,j}^{chg} = SoC_{t,j} - SoC_{t-d,j} \tag{2}$$

The proposed strategy assigns a priority level $L_{t,j}$ to the j^{th} EV at time step t according to:

$$L_{t,j} = \begin{cases} 1 & W_{t,j}^{chg} < \phi \\ 2 & \phi \le W_{t,j}^{chg} < 2\phi \\ \vdots & \\ \lambda & (\lambda-1)\phi \le W_{t,j}^{chg} < \lambda\phi \end{cases} \tag{3}$$

where λ is the number of priority levels in the system that can be assigned to EVs; and ϕ is the total SoC increase that moves an EV from one priority level to another. The priority level is updated at each time step t. In (3), $L_{t,j}=1$ is a higher priority level than $L_{t,j}=2$ because that latter has gained higher SoC in the past time horizon. In summary, the priority system embedded in each local charger uses the SoC increase of EV battery in the historical time horizon to assign an EV a priority level without the need for communication with system operator or other chargers. The priority level will affect the charging power that an EV is allocated through the adjustable parameter in Sigmoid-based controller as explained in the next subsection.

B. Sigmoid-based Controller

A Sigmoid-based controller is programmed on each EV charger. The EV charging power is controlled based on the adaptive charging speed factor $H_{t,j}$, which is a multiplication of Sigmoid-based functions of voltage and frequency, as given by:

$$H_{t,j} = \frac{1}{1+\mathrm{e}^{-\rho(L_{t,j})v_{t,j}}} \frac{1}{1+\mathrm{e}^{-\rho(L_{t,j})f_{t,j}}} \tag{4}$$

where $v_{t,j}$ and $f_{t,j}$ are the voltage and frequency measured by the charger at the PCC, respectively; and $\rho(\cdot)$ is a function of the priority level $L_{t,j}$. Equation (4) consists of two Sigmoid-based functions multiplied by each other. The first function changes in response to the changes in $v_{t,j}$ at time step t, while the second function is changed according to $f_{t,j}$. The parameter ρ in (4) changes according to the priority level $L_{t,j}$ of the EV. This parameter affects the rate of change of the Sigmoid-based functions, i.e., the shape and rise of the function. In this context, a lower priority level for an EV indicates that a decrease in frequency or voltage will result in a higher reduction of charging speed in comparison to higher priority EVs. The effect of the priority level on the level of charging speed reduction in the frequency-based control function is demonstrated in Fig. 2. As shown in this figure, the decrease in the priority level from level 1 ($L=1$) to level 6 ($L=6$) increases the decay rate of the function in response to the decrease of system frequency and, therefore, slows the EV charging speed. The voltage-based control function has a similar behavior but with an input range corresponding to voltage measurements. In this study, it is proposed that the setting of parameter ρ is based on providing high reduction in the charging speed for the lower priority levels and slight reduction to higher priority levels in the event that system parameters, i.e., system frequencies and/or bus voltages, decrease from their nominal values. Once system frequencies and /or bus voltages are in the intermediate region between their nominal value and lower limit, the function should start to steeply reduce the EV charging speed from all priority levels, albeit keeping the higher charging rate for higher priority levels. When system parameters are close to their lower limits, the charging power reduction is almost equal for all priority levels.

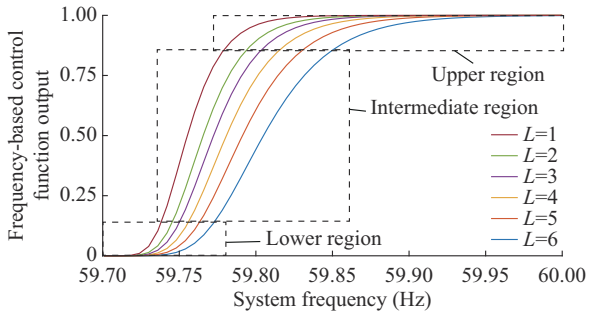

Fig. 2. Example of how EV charging speed for frequency-based control function varies with priority level.

The Sigmoid-based controller is utilized in the proposed strategy because it provides three regions of continuous EV charging control, as illustrated in Fig. 2. Under nominal system operation condition (system frequencies and/or bus voltages are 1 p.u.), the EV charging speed factor is set at unity, i.e., EV charges at full speed. When the deviation for the system operation from the nominal values is small (upper region), the EV charging speed decreases slowly. This prevents unnecessary reduction of charging power when the system operating parameter is slightly deviating from its nominal value. The intermediate region provides a rapid reduction in the charging speed to slow the decrease in system frequencies and/or bus voltages. When the system parameter is near its acceptable lower limit in the lower control region, the charging speed is slowly changed to prevent any large power oscillation near this point in case of synchronized actions of controllers. For example, if the system parameter is increasing in the lower region, the charging speed factor is slowly increased to ensure that the power system can handle the extra load without putting its stability at risk.

C. Charging Current Calculation

The charging current of the j^{th} EV at each time step t is determined by:

$$I_{t,j}^{Batt} = I_j^{\max} \quad SoC_{t,j} < SoC_j^{\min} \tag{5}$$

$$I_{t,j}^{Batt} = I_j^{\min} + (I_j^{\max} - I_j^{\min})H_{t,j} \quad SoC_j^{\min} \le SoC_{t,j} < SoC_j^{\max} \tag{6}$$

$$I_{t,j}^{Batt} = 0 \quad SoC_{t,j} \ge SoC_j^{\max} \tag{7}$$

where $I_j^{\min}$ and $I_j^{\max}$ are the minimum and the maximum output current limits of the charger for the j^{th} EV, respectively; and $SoC_j^{\min}$ and $SoC_j^{\max}$ are the minimum and the maximum limits of SoC for the j^{th} EV, respectively. A minimum charg-

ing current is included based on the requirements of EV charging standards [28]. In summary, when $SoC_{t,j}$ is below the pre-defined minimum limit $SoC_j^{\min}$, the EV charger provides the maximum charging current to the EV battery. When $SoC_{t,j}$ is below the maximum limit but above the minimum limit, the proposed strategy adjusts the charging current based on the Sigmoid-based controller represented by $H_{t,j}$ calculated in (4). If $SoC_{t,j}$ is higher than the maximum limit $SoC_j^{\max}$, the strategy switches off the EV charger to preserve the battery lifetime.

D. Communication-less EV Load Shedding Scheme

In the situations where the system frequencies and/or bus voltages go below their respective lower limit despite the reduction of the EV charging current to the minimum, the proposed strategy can deactivate the EV charger through its shedding scheme. While the EV is plugged in, a communication-less EV load shedding scheme continuously monitors the system frequency, bus voltage, and EV priority level at each time step t, as shown in Fig. 1. Based on these inputs, the scheme decides the charger status through the shedding control signal $K_{t,j}$, where $K_{t,j}=0$ deactivates the charger. Figure 3 and Algorithm 1 demonstrate the overall logic of the proposed comunication-less EV load shedding scheme.

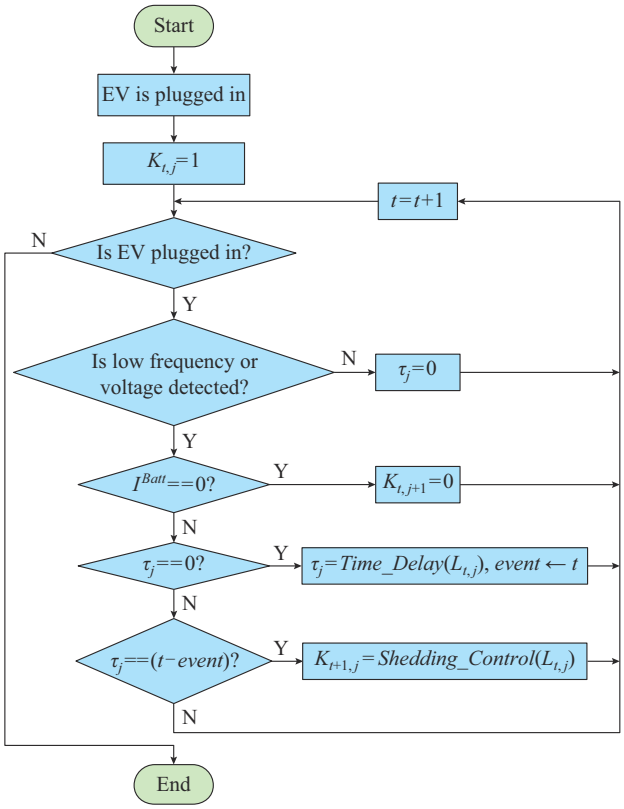

Fig. 3. Flow chart of proposed communication-less EV load shedding scheme.

By default, $K_{t,j}=1$ for any time step unless it is changed by the load shedding scheme. When the system frequencies or the bus voltages go below their respective acceptable limit f_r or v_r, the load shedding scheme checks whether the EV is being charged at the current time step t.

Algorithm 1: proposed communication-less EV load shedding scheme

Input: priority level $L_{t,j}$, system frequencies f_t, and bus voltages $v_{t,j}$ measured at the j^{th} EV PCC

Output: shedding control signal $K_{t,j}$

$K_{t,j} \leftarrow 1 ; \forall t$

Function Main ($f_{t,j}$, $v_{t,j}$, $L_{t,j}$)

```
while EV is plugged in do
  if f_{t,j} < f_r or v_{t,j} < v_r then
    if I^{Batt}_{t,j} == 0 then
      K_{t+1,j} = 0
    else
      if τ_j == 0 then
        τ_j = Time_Delay(L_{t,j})
        event ← t
      else
        if τ_j == (t − event) then
          K_{t+1,j} = Shedding_Control(L_{t,j})
  else
    τ_j = 0
```

If the EV is charging, the EV is assigned a time delay τ_j based on the function *Time_Delay*, which is detailed in Algorithm 2. The purpose of the time delay is to wait for the system frequencies and/or bus voltages to return to their normal operation range and prevent nuisance load shedding. The time delay assigned by this function varies according to the priority level assigned to the EV at that particular time step. In this regard, EVs with lower priority levels are assigned shorter time delays to be shed. It is worth noting that the function *Time_Delay* assigns random time delays within a certain range for each priority level. This prevents the simultaneous shedding of EVs that belong to the same priority level, which could lead to large swings in the system load that affects its stability. In case an EV is not charging because it has been deactivated by a previous shedding control signal, the proposed scheme will not make any change and the shedding signal for the next time step is kept at zero. In a situation where a time delay is assigned, the proposed scheme checks if the time delay has passed based on the recorded *event* time. In that case, the function *Shedding_Control* in Algorithm 3 deactivates the charger for a future time set Δ based on the priority level. The deactivation time, i.e., the total time in which the charger is switched off, increases as the priority level decreases. In Algorithm 3, x_1 and x_2 are the deactivation time adjustment variables.

Algorithm 2: time delay function

Function *Time_Delay*($L_{t,j}$)

```
if L_{t,j} == 1 then
  τ_j = rand(π, 2π)
else if L_{t,j} == 2 then
  τ_j = rand(2π, 3π)
  ⋮
else if L_{t,j} == λ then
  τ_j = rand(λπ, (λ + 1)π)
```

Algorithm 3: shedding control function

Function *Shedding_Control*($L_{t,j}$)

if $L_{t,j}==\lambda$ **then**

$\Delta_1=[t+x_1, t+x_2]$

$K_{\Delta_1,j}=0$

else if $L_{t,j}==\lambda-1$ **then**

$\Delta_2=[t+x_2, t+x_3]$

$K_{\Delta_2,j}=0$

⋮

else if $L_{t,j}==1$ **then**

$K_{\Delta_1,j}=0$

E. Performance Index

The effectiveness of the proposed strategy to reduce the violations of the system operation constraints that result from EV charging is quantified using the SVI as:

$$SVI=\sum_{t\in T}\left|\Omega_t^f\right|\Delta t+\sum_{i\in\mathbb{B}}\sum_{t\in T}\left|\Omega_{t,i}^v\right|\Delta t \quad \forall t\in T\wedge\forall i\in\mathbb{B} \tag{8}$$

$$\Omega_t^f=\begin{cases}f_t-f_{ru} & f_t>f_{ru}\\ f_{rl}-f_t & f_t<f_{rl}\\ 0 & \text{else}\end{cases} \tag{9}$$

$$\Omega_{t,i}^v=\begin{cases}v_{t,i}-v_{ru} & v_{t,i}>v_{ru}\\ v_{rl}-v_{t,i} & v_{t,i}<v_{rl}\\ 0 & \text{else}\end{cases} \tag{10}$$

where Ω_t^f and $\Omega_{t,i}^v$ are the frequency and voltage violation factors, respectively; Δt is the time step; f_{rl} and v_{rl} are the parameters representing the minimum operation limits for system frequencies and bus voltages, respectively; f_{ru} and v_{ru} are the maximum limits for system frequencies and bus voltages, respectively; $\mathbb{B}$ is the set of buses in the power system; and T is the set of time steps in the studied duration. The acceptable frequency limit is typically within the range of $f_{rl}=$ 59.70 Hz to $f_{ru}=60.3$ Hz, while the acceptable voltage limit is usually within $v_{rl}=0.95$ p.u. to $v_{ru}=1.05$ p.u.. These values define the operation boundaries for system frequencies and bus voltages to ensure the stability and reliability of the power system [29], [30].

III. Test Model of Droop-based IMG

In IMGs, DGs are the main components responsible for creating balanced power generation in the distribution systems [31]. Due to the absence of a slack bus, DGs are operated to follow the power demand by controlling the system frequencies and bus voltages of the IMG system. Therefore, the suitable operation mode for DGs is the droop control, where without loss of generality, the injected active power $P_{i,t}^{Src}$ increases by drooping the frequency of the DG unit output voltage, and the reactive power $Q_{i,t}^{Src}$ increases by drooping the magnitude of the DG unit output voltage as [17]:

$$P_{i,t}^{Src}=\frac{\omega_i^*-\omega_t}{m_{P_{i,t}}} \quad \forall i\in\mathbb{G},\mathbb{G}\subseteq\mathbb{B} \tag{11}$$

$$Q_{i,t}^{Src}=\frac{\left|V_i^*\right|-\left|V_{i,t}\right|}{n_{q_{i,t}}} \quad \forall i\in\mathbb{G}\subseteq\mathbb{B} \tag{12}$$

where $m_{P_{i,t}}$ and $n_{q_{i,t}}$ are the droop control settings for DG i; ω_i^* is the frequency set for the DG with no load; $\left|V_i^*\right|$ is the voltage at no load for the DG; $\left|V_{i,t}\right|$ is the voltage of the bus connected to the DG; ω_t is the system operation frequency at time step t; and $\mathbb{G}$ is a subset of buses with DGs. The drooped injected active power and reactive power are balanced with the load demands $P_{i,t}^{Dmd}$ and $Q_{i,t}^{Dmd}$ through the power mismatch equations as:

$$\sum_{l\in\mathbb{B}}\left(\left|V_{i,t}\right|\left|V_{l,t}\right|Y_{il}\cos(\theta_{il}+\delta_{l,t}-\delta_{i,t})\right)=P_{i,t}^{Src}-P_{i,t}^{Dmd} \quad \forall i,l\in\mathbb{B}\wedge i\neq l \tag{13}$$

$$\sum_{l\in\mathbb{B}}\left|V_{i,t}\right|\left|V_{l,t}\right|Y_{il}\sin(\theta_{il}+\delta_{l,t}-\delta_{i,t})=Q_{i,t}^{Src}+Q_{i,t}^{Dmd} \quad \forall i,l\in\mathbb{B}\wedge i\neq l \tag{14}$$

where Y_{il} and θ_{il} are the Y-bus admittance magnitude and angle, respectively; and $\delta_{l,t}$ and $\delta_{i,t}$ are the voltage phase angle at any bus l and bus i at time step t, respectively.

IV. Numerical Simulations

Numerical simulations are performed in a MATLAB environment to test the effectiveness of the proposed strategy. The modified IEEE 33-bus test IMG system shown in Fig. 4(a) is selected as the test system [32]. The power distribution system operates as an IMG and consists of a 33-bus primary distribution network operating at a nominal voltage of 12.47 kV. In order to capture the interaction of IMG with EV chargers installed in residential areas, seven secondary distribution networks operating at 220 V are modeled and connected to the primary buses. Each secondary distribution network is modeled as per the CIGRE 14-node residential lateral benchmark containing lines 1-14 (L1-L14), as shown in Fig. 4(b) [33]. Non-EV residential load profiles with a resolution of 1 min are generated from real data of houses in Canada [34]. It is assumed that a total of four DGs are connected in the system, where all the DGs are dispatchable with the exception of DG2, which is wind-powered. The DG parameters in IEEE 33-bus test IMG system including ratings, droop, and nominal operation settings are listed in Table I, where S_{gmax} is the MVA rating of DG. The wind power profile for DG2 is shown in Fig. 5 [35].

Level-2 chargers with a maximum charging power of 6.6 kW are considered in this study, and the minimum charging rate is set to be 1.5 kW as per the IEC 61851 standard. A maximum of 200 EVs are assumed to be present in the IMG system, which sets the rated EV charging load to be around 35% of the total rated system load. The battery capacities for all EVs are set to be 62 kWh, which are similar to those of the Tesla Model 3, one of the most popular EVs in the market [36]. $SoC^{\min}$ and $SoC^{\max}$ are set to be 25% and 85%, respectively. The EVs are assumed to be charged at homes while the arrival time follows a truncated Gaussian distribution with a mean value μ of 5 p.m. and a standard deviation σ of 1.5 hours [37].

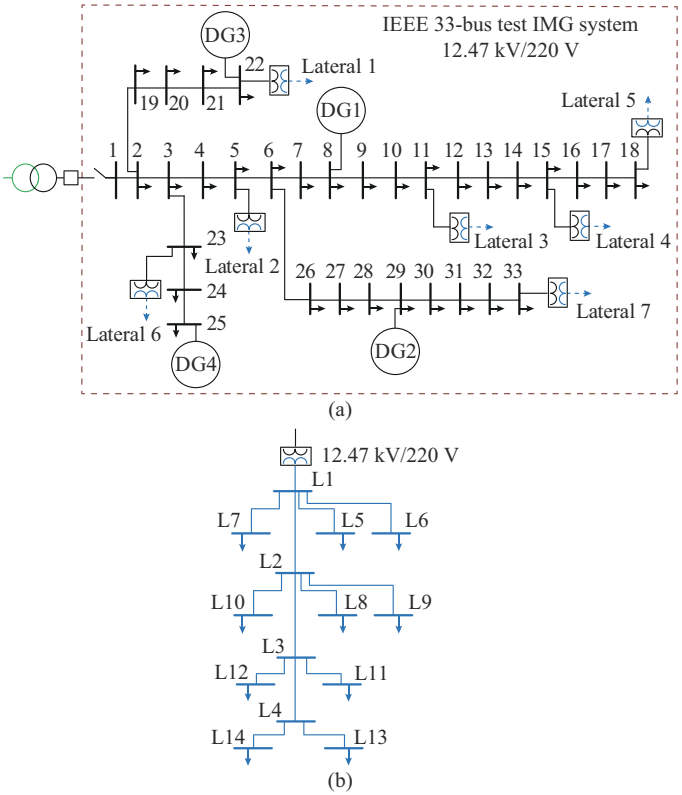

Fig. 4. Test IMG system. (a) IEEE 33-bus test IMG system. (b) CIGRE 14-node secondary network.

TABLE I
DG PARAMETERS IN IEEE 33-BUS TEST IMG SYSTEM

DG No.	m_P (p.u.)	n_q (p.u.)	ω^* (p.u.)	V^* (p.u.)	S_{gmax} (MVA)	Power factor
1	0.00208	0.0486	1	1.03	2.5	0.80
2					1.5	0.95
3	0.00505	0.1010	1	1.02	1.0	0.80
4	0.00833	0.1660	1	1.02	0.6	0.80

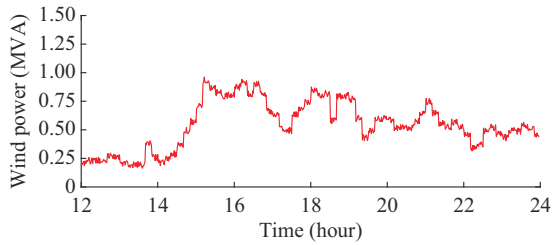

Fig. 5. Wind power profile for DG2.

The initial battery SoCs of EVs at arrival follow a Gaussian distribution with $\mu = 45\%$ and $\sigma = 10\%$. All case studies are run from 12 p.m. to 12 a.m.. The time interval of simulation studies is 1 min. Without loss of generality, six priority levels are chosen based on $d = 6$ hours and ϕ. The parameters of Sigmoid-based controller are listed in Table II. These parameters are chosen based on six priority levels to create a control that varies when bus voltages and system frequencies go below 1 p.u. and 60 Hz, respectively. The level of variation between the priority levels is guided by the objectives that include the grid stability and minimal power system impact during EV charging. Throughout the parameter tuning process, trade-off considerations between different performance objectives are carefully examined to address the challenges of achieving a stable charging system. By iteratively adjusting and fine-tuning the parameters based on simulation outcomes, ρ is determined.

TABLE II
PARAMETERS OF SIGMOID-BASED CONTROLLER

Level	ρ	Level	ρ
*L*6	2000	*L*3	2900
*L*5	2300	*L*2	3200
*L*4	2600	*L*1	3500

It should be noted that *Lx* in Table II and the following figures refers to priority level $L = x$, e.g., *L*6 means $L = 6$.

A. System Operation Without EV

In case 1, the IMG is run without the presence of EV loads. Figure 6(a) and (b) shows the bus voltages and system frequencies, respectively, while the normal load power is shown in Fig. 6(c).

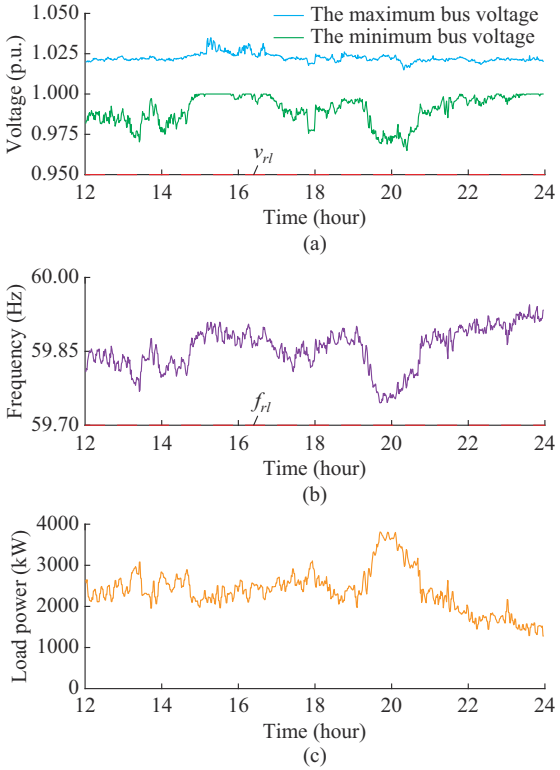

Fig. 6. Simulation results of case 1. (a) The minimum and maximum bus voltages. (b) System frequencies. (c) Normal load power.

Active and reactive power outputs of DG are shown in Fig. 7(a) and (b), respectively. It is noticed from Fig. 6(a) and (b) that the bus voltages and system frequencies are within the standard limits, which specify that the acceptable operation ranges for bus voltages and system frequencies are

between 0.95 p.u. and 1.05 p.u., and 0.995 p.u. (59.7 Hz) to 1.005 p.u. (60.3 Hz), respectively [38]. Both the bus voltages and system frequencies reach their lowest operation points when the normal load power peaks around 8 p.m., as demonstrated in Fig. 6(c).

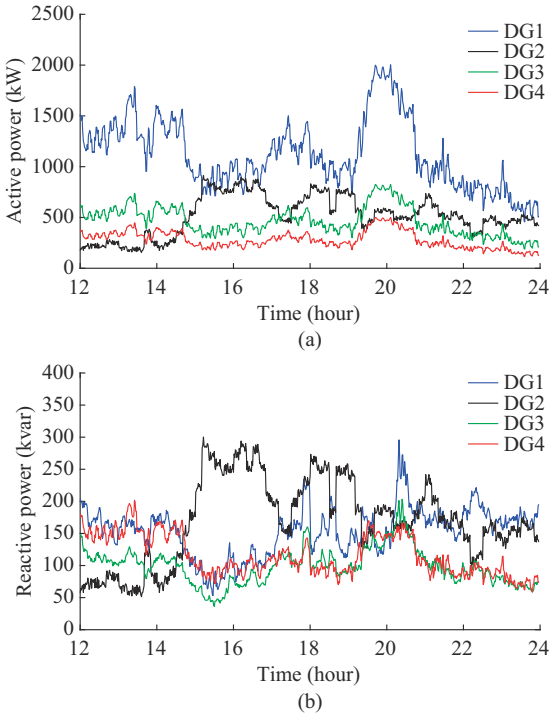

Fig. 7. Active and reactive power of DGs. (a) Active power. (b) Reactive power.

B. Opportunistic Charging

In case 2, the IMG is simulated with the presence of EV load and the assumption that the EVs charge at their available rated power. Figure 8(a)-(d) demonstrates the operation parameters for this case. It is clear from Fig. 8(a) and (b) that no violation is recorded in system parameters under light loading conditions. However, this type of EV charging results in an unacceptable violation of the respective limits of both the bus voltages and system frequencies during the peak load time. The voltage limit violations occur in laterals 4 and 5 because they are relatively farther from the nearest DGs than other laterals. It is noteworthy that these violations result from the coincidence of both normal and EV peak loads. These conditions overload the DGs in the IMG and cause undesirable voltage drops across the distribution lines.

C. Controlled Charging

1) Proposed Strategy Versus Voltage-based Controller

The proposed strategy in Section II is simulated and compared with controllers from the state-of-the-art review. First, the proposed strategy is compared with the voltage-based controller proposed in [25]. The charging controller proposed in [25] is given by:

$$EP_{t,j}=\begin{cases}P_j^{\min}+\beta_j e^{-u_{j,i}(v_{t,j}-v_{ru})}e^{1-SoC_{t,j}} & v_{t,j}\geq v_{rl}\\ 0 & v_{t,j}<v_{rl}\end{cases} \quad (15)$$

where $EP_{t,j}$ is the charger power; $P_j^{\min}$ is the minimum charger power; β_j is a controller parameter for the j^{th} EV; and $u_{t,j}$ is the sensitivity measured by the charger of the j^{th} EV. v_{rl} in (15) is a reference voltage set to the lower acceptable limit, which is 0.95 p.u..

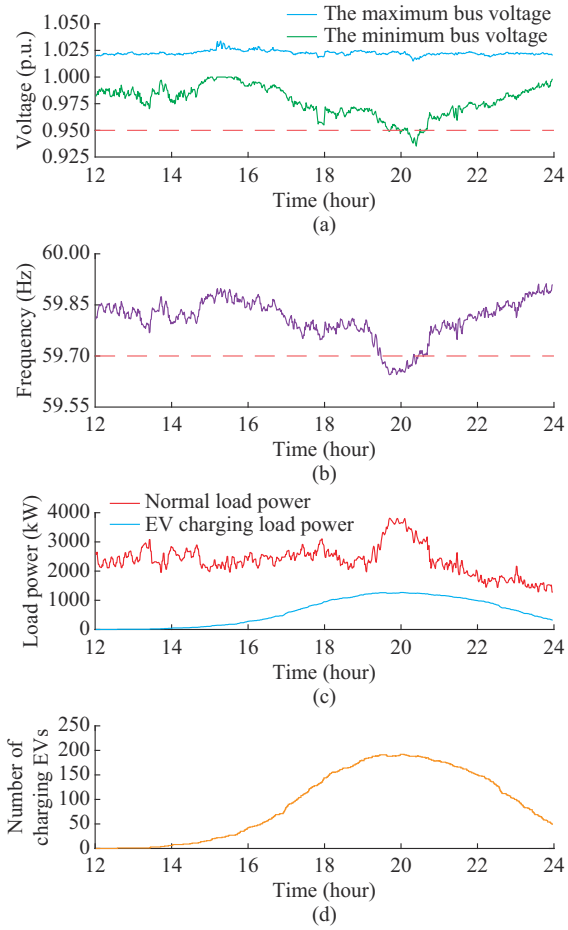

Fig. 8. Simulation results of case 2. (a) The minimum and maximum bus voltages. (b) System frequency. (c) Normal and EV charging load power. (d) Number of charging EVs.

The performances of the two controllers during peak load period from the 19th to 21st hours are compared to test their effectiveness in controlling the EV charging load when system operation parameters approach their lower respective limits. Simulation results for the voltage-based controller are shown in Fig. 9(a)-(c). Figure 9(a) shows that the voltage-based controller results in oscillations around the lower limit of voltage during the peak load period. These oscillations occur because of the discontinuity in the controller that leads to charging load fluctuations, as shown in Fig. 9(c). It is worth to recall that this controller is designed to control EV charging based on voltage, and therefore, the frequency violation shown in Fig. 9(b) is not corrected due to the absence of frequency in the input parameters of the controller. The results of the proposed strategy are demonstrated in Fig. 9(d)-(f). Figure 9(d) and (e) shows that the bus voltages and system frequencies stay above their respective lower limits under the peak load conditions. This is because each EV charger in the system modulates its power according to the mea-

sured voltage and frequency. This results in reduced total EV charging load, as shown in Fig. 9(f), which relieves the DGs and reduces voltage drops across the system. It is also important to note that in contrast to previous research works, the charging fairness technique implemented in the proposed strategy does not degrade the performance of the EV charging control. Figure 9(a) and (c) shows that the EV charging load for the voltage-based controller slightly changes in response to voltage changes due to the presence of sensitivity parameter that is used to achieve charging fairness. Meanwhile, the proposed strategy effectively controls the EV charging according to system conditions, as shown in Fig. 9(d)-(f).

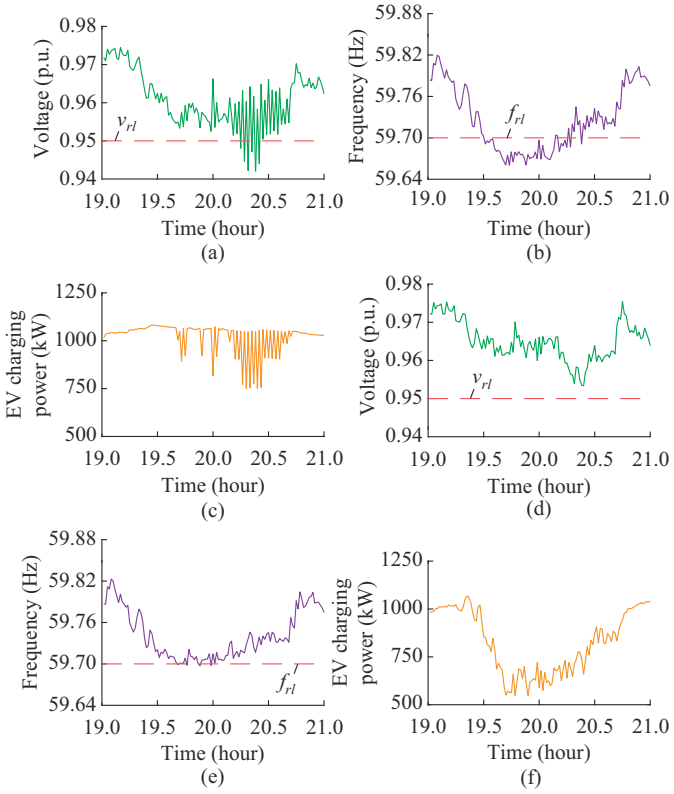

Fig. 9. Simulation results for voltage-based controller and proposed strategy during peak load period. (a) The minimum bus voltage for voltage-based controller. (b) System frequency for voltage-based controller. (c) EV charging power for voltage-based controller. (d) The minimum bus voltage for proposed strategy. (e) System frequency for proposed strategy. (f) EV charging power for proposed strategy.

The SVI for opportunistic charging, voltage-based controller, and proposed strategy are listed in Table III. It can be observed that the proposed strategy provides a remarkable improvement in reducing violations of system parameters.

TABLE III
SVI FOR DIFFERENT CHARGING TECHNIQUES

Technique	SVI
Opportunistic charging	0.0855
Voltage-based controller	0.0196
Proposed strategy	0

As described in Section II, the level at which charging power is reduced depends on those of each EV. Figure 10 presents the priority level distribution of EV during peak load period for the proposed strategy and demonstrates the power system capacity allocation for different priority levels. It is clear from the figure that a higher priority level (less past charging allocation) will result in higher power allocation for the EV.

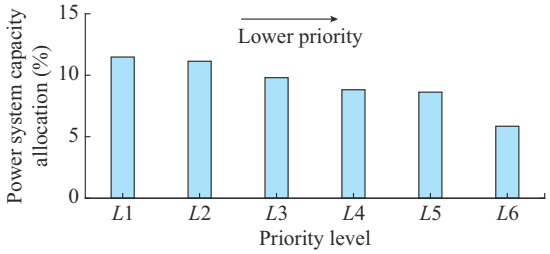

Fig. 10. Priority level distribution of EV during peak load period for proposed strategy.

2) Proposed Strategy Versus Frequency-based Controller

The proposed strategy is also compared with the frequency-based controller implemented in [18], which is represented by:

$$I_{t,j}^{Batt} = I_j^{\min} + (I_j^{\max} - I_j^{\min})(f_t - f_{rl})\Psi \tag{16}$$

where Ψ is the controller droop gain. Figure 11 demonstrate the system parameters during peak load period when the frequency-based controller is implemented in the IMG. As noticed from Fig. 11, the controller helps avoid violations in the system frequencies and bus voltages during the peak period.

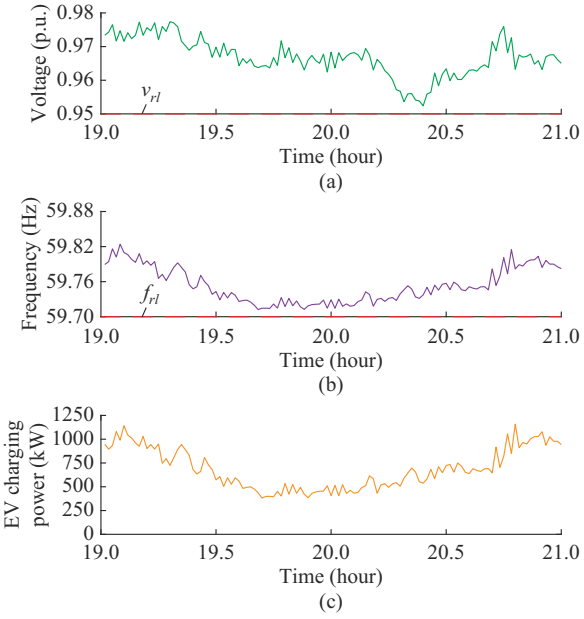

Fig. 11. Simulation results for frequency-based controller during peak load period. (a) The minimum bus voltage. (b) System frequencies. (c) EV charging power.

Nonetheless, the controller applies equal charging reduction to all EVs without consideration of fairness, as can be observed from Fig. 12, which shows the charging power allocation during the peak load period for the frequency-based controller.

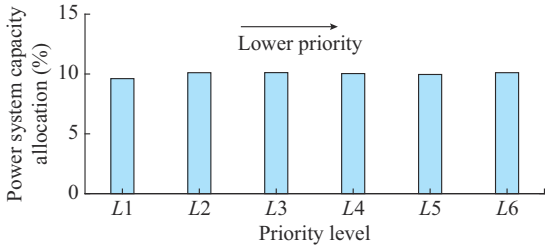

Fig. 12. Priority level distribution of EV during peak load period for frequency-based controller.

The performances of the frequency-based controller and the proposed strategy are also compared during DG outages, which could cause a further drop in system frequency during the peak load period. A DG outage scenario is implemented where DG4 goes out of service at 6:30 p.m.. Figure 13(a)-(c) illustrates the results for this scenario in the case of the frequency-based controller. Figure 13(a)-(c) shows oscillations in bus voltages, system frequencies, and EV charging power when the DG outage event occurs during the peak load period. These oscillations occur despite the reduction of charging load to the minimum limit, as shown in Fig. 13(c), which indicates that further curtailment of EV load is required.

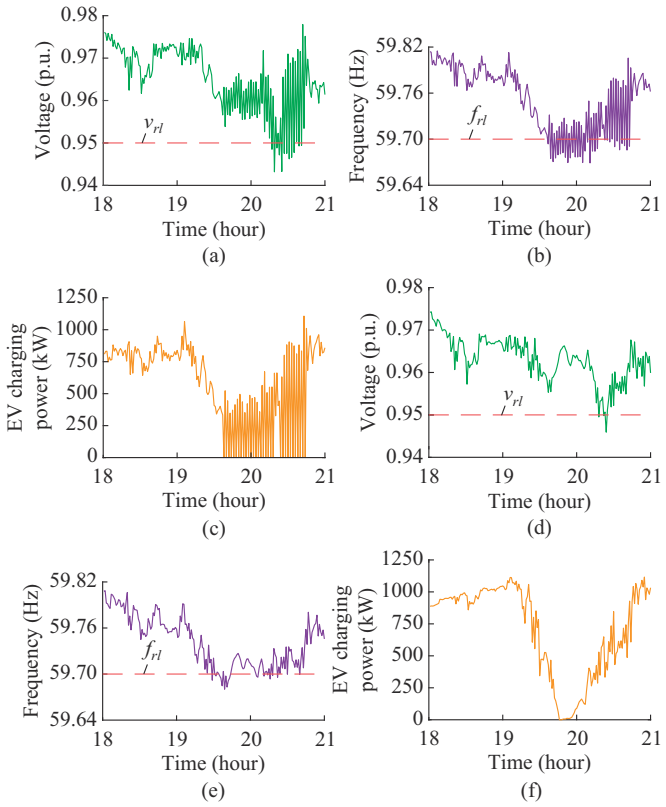

Fig. 13. Simulation results of frequency-based controller and proposed strategy in DG outage scenario. (a) The minimum bus voltage for frequency-based controller. (b) System frequencies for frequency-based controller. (c) EV charging power for frequency-based controller. (d) The minimum bus voltage for proposed strategy. (e) System frequencies for proposed strategy. (f) EV charging power for proposed strategy.

The simulation results of DG4 outage scenario are demonstrated in Fig. 13(d)-(e) for the proposed strategy. It is worth noting that once the shedding scheme detects a violation of bus voltages and system frequencies, it starts to curtail EV loads to prevent further violations and bring back the system parameters to the acceptable limits, as shown in Fig. 13(d) and (e). This would, in turn, result in shifting the peak EV charging load a bit further and relieve the system under the abnormal condition of the DG outage, as demonstrated in Fig. 13(f).

The SVI for this scenario is calculated for the frequency-based controller and the proposed strategy, as shown in Table IV. The values of SVI indicate that the load shedding scheme incorporated in the proposed strategy greatly reduces the system parameter violations during the DG outage.

TABLE IV
SVI FOR FREQUENCY-BASED CONTROLLER AND PROPOSED STRATEGY IN A DG OUTAGE SCENARIO

Technique	SVI
Frequency-based	0.0247
Proposed strategy	0.0039

V. CONCLUSION

This study develops a communication-less management strategy for the EV charging in droop-controlled IMGs. The proposed strategy controls the EV charging rate based on both the system frequencies and bus voltages as well as the past charging power allocation. Further, a charging fairness system that assigns priority levels to EVs based on their past charging power allocation is developed. Moreover, a novel communication-less EV load shedding scheme is proposed that gets triggered when an under-voltage or under-frequency event occurs in the IMG. Numerical simulations are conducted to validate the effectiveness of the proposed strategy. The results demonstrate the superiority of the proposed strategy to the state-of-the-art controllers in modulating the EV charging load. The results also show that the charging fairness system implemented in the proposed strategy does not degrade the performance of the EV charging control. During a DG outage scenario, the proposed strategy successfully curtailed EV loads to prevent further violations and bring back the system operation parameters to acceptable limits. The effectiveness of the proposed strategy in controlling EV charging without the presence of communication is significant because it introduces an implementable and cost-effective solution that reduces the anticipated upgrades in power systems that are required for the seamless integration of EVs.

In future, optimizing the values of d and ρ can be a focus of research to enhance the effectiveness of the control strategy. Advanced machine learning techniques could be involved to analyze historical data and identify patterns in EV charging behavior that have the most significant impact on grid stability.

REFERENCES

[1] S. Alshahrani, M. Khalid, and M. Almuhaini, "Electric vehicles beyond energy storage and modern power networks: challenges and applications," *IEEE Access*, vol. 7, pp. 99031-99064, Jun. 2019.
[2] Y. Yu, D. Reihs, S. Wagh *et al.*, "Data-driven study of low voltage dis-

tribution grid behaviour with increasing electric vehicle penetration," *IEEE Access*, vol. 10, pp. 6053-6070, Oct. 2022.
[3] J. Pahasa and I. Ngamroo, "Coordinated PHEV, PV, and ESS for microgrid frequency regulation using centralized model predictive control considering variation of PHEV number," *IEEE Access*, vol. 6, pp. 69151-69161, Jun. 2018.
[4] M. Ahmed, Y. Abouelseoud, N. H. Abbasy *et al*., "Hierarchical distributed framework for optimal dynamic load management of electric vehicles with vehicle-to-grid technology," *IEEE Access*, vol. 9, pp. 164643-164658, 2021.
[5] A. Al-Obaidi, H. Khani, H. E. Z. Farag *et al*., "Bidirectional smart charging of electric vehicles considering user preferences, peer to peer energy trade, and provision of grid ancillary services," *International Journal of Electrical Power & Energy Systems*, vol. 124, p. 106353, Jan. 2021.
[6] M. F. M. Arani and Y. A. R I. Mohamed, "Cooperative control of wind power generator and electric vehicles for microgrid primary frequency regulation," *IEEE Transactions on Smart Grid*, vol. 9, no. 6, pp. 5677-5686, Nov. 2018.
[7] P. Kou, D. Liang, R. Gao *et al*., "Decentralized model predictive control of hybrid distribution transformers for voltage regulation in active distribution networks," *IEEE Transactions on Sustainable Energy*, vol. 11, no. 4, pp. 2189-2200, Oct. 2020.
[8] A. Zahedmanesh, D. Sutanto, and K. M. Muttaqi, "Analyzing the impacts of charging plug-in electric vehicles in low voltage distribution networks: a case study of utilization of droop charging control system based on the SAE J1772 Standard," in *Proceedings of 2017 Australasian Universities Power Engineering Conference (AUPEC)*, Melbourne, Australia, Nov. 2017, pp. 1-6.
[9] L. Xia, I. Mareels, T. Alpcan *et al*., "A distributed electric vehicle charging management algorithm using only local measurements," in *Proceedings of Innovative Smart Grid Technologies*, Washington DC, USA, Feb. 2014, pp. 1-5.
[10] A. C. Melhorn, K. McKenna, A. Keane *et al.*, "Autonomous plug and play electric vehicle charging scenarios including reactive power provision: a probabilistic load flow analysis," *IET Generation, Transmission & Distribution*, vol. 11, no. 3, pp. 768-775, Feb. 2017.
[11] M. H. Mobarak and J. Bauman, "Vehicle-directed smart charging strategies to mitigate the effect of long-range EV charging on distribution transformer aging," *IEEE Transactions on Transportation Electrification*, vol. 5, no. 4, pp. 1097-1111, Dec. 2019.
[12] J. E. Cardona, J. C. López, and M. J. Rider, "Decentralized electric vehicles charging coordination using only local voltage magnitude measurements," *Electric Power Systems Research*, vol. 161, pp. 139-151, Aug. 2018.
[13] P. Richardson, D. Flynn, and A. Keane, "Local versus centralized charging strategies for electric vehicles in low voltage distribution systems," *IEEE Transactions on Smart Grid*, vol. 3, no. 2, pp. 1020-1028, Jun. 2012.
[14] S. Faddel, T. Youssef, A. T. Elsayed *et al*., "An automated charger for large-scale adoption of electric vehicles," *IEEE Transactions on Transportation Electrification*, vol. 4, no. 4, pp. 971-984, Dec. 2018.
[15] A. T. Al-Awami, E. Sortomme, G. M. A. Akhtar *et al*., "A voltage-based controller for an electric-vehicle charger," *IEEE Transactions on Vehicular Technology*, vol. 65, no. 6, pp. 4185-4196, Jun. 2016.
[16] M. Singh, P. Kumar, and I. Kar, "Implementation of vehicle to grid infrastructure using fuzzy logic controller," *IEEE Transactions on Smart Grid*, vol. 3, no. 1, pp. 565-577, Mar. 2012.
[17] M. M. A. Abdelaziz, H. E. Farag, E. F. El-Saadany *et al*., "A novel and generalized three-phase power flow algorithm for islanded microgrids using a Newton trust region method," *IEEE Transactions on Power Systems*, vol. 28, no. 1, pp. 190-201, Feb. 2013.
[18] Y. Ota, H. Taniguchi, J. Baba *et al*., "Implementation of autonomous distributed V2G to electric vehicle and DC charging system," *Electric Power Systems Research*, vol. 120, pp. 177-183, Mar. 2015.
[19] M. Tokudome, K. Tanaka, T. Senjyu *et al*., "Frequency and voltage control of small power systems by decentralized controllable loads," in *Proceedings of 2009 International Conference on Power Electronics and Drive Systems* (*PEDS*), Taipei, China, Nov. 2009, pp. 666-671.
[20] M. Zeballos, A. Ferragut, and F. Paganini, "Proportional fairness for EV charging in overload," *IEEE Transactions on Smart Grid*, vol. 10, no. 6, pp. 6792-6801, Nov. 2019.
[21] Z. Fan, "A distributed demand response algorithm and its application to PHEV charging in smart grids," *IEEE Transactions on Smart Grid*, vol. 3, no. 3, pp. 1280-1290, Sept. 2012.
[22] N. Rahbari-Asr and M. Y. Chow, "Cooperative distributed demand management for community charging of PHEV/PEVs based on KKT conditions and consensus networks," *IEEE Transactions on Industrial Informatics*, vol. 10, no. 3, pp. 1907-1916, Aug. 2014.
[23] G. Binetti, A. Davoudi, D. Naso *et al*., "Scalable real-time electric vehicles charging with discrete charging rates," *IEEE Transactions on Smart Grid*, vol. 6, no. 5, pp. 2211-2220, Sept. 2015.
[24] N. I. Nimalsiri, C. P. Mediwaththe, E. L. Ratnam *et al*., "A survey of algorithms for distributed charging control of electric vehicles in smart grid," *IEEE Transactions on Intelligent Transportation Systems*, vol. 21, no. 11, pp. 4497-4515, Nov. 2020.
[25] S. Shafiq and A. T. Al-Awami, "An autonomous charge controller for electric vehicles using online sensitivity estimation," *IEEE Transactions on Industry Applications*, vol. 56, no. 1, pp. 22-33, Jan. 2020.
[26] S. Tang, Z. Niu, B. He *et al*., "Long-term multi-resource fairness for pay-as-you use computing systems," *IEEE Transactions on Parallel and Distributed Systems*, vol. 29, no. 5, pp. 1147-1160, May 2018.
[27] E. Inoa and J. Wang, "PHEV charging strategies for maximized energy saving," *IEEE Transactions on Vehicular Technology*, vol. 60, no. 7, pp. 2978-2986, Sept. 2011.
[28] International Electrotechnical Commission. (2017, Jan.). Electric vehicle conductive charging system–part 1: general requirements. [Online]. Available: https://webstore.iec.ch/publication/33644.
[29] NERC. (2023, Jul.). NERC interconnection frequency response. [Online]. Available: https://www. nerc. com/pa/RAPA/ri/Pages/InterconnectionFrequencyResponse.aspx
[30] P. T. Ogunboyo, R. Tiako, and I. E. Davidson, "Effectiveness of dynamic voltage restorer for unbalance voltage mitigation and voltage profile improvement in secondary distribution system," *Canadian Journal of Electrical and Computer Engineering*, vol. 41, no. 2, pp. 105-115, Apr. 2018.
[31] M. F. Ishraque, S. A. Shezan, M. M. Ali *et al*., "Optimization of load dispatch strategies for an islanded microgrid connected with renewable energy sources," *Applied Energy*, vol. 292, p. 116879, Jun. 2021.
[32] M. E. Baran and F. Wu, "Network reconfiguration in distribution systems for loss reduction and load balancing," *IEEE Transactions on Power Delivery*, vol. 4, no. 2, pp. 1401-1407, Apr. 1989.
[33] K. Strunz, R. H. Fletcher, R. Campbell *et al*., "Developing benchmark models for low-voltage distribution feeders," in *Proceedings of 2009 IEEE PES General Meeting*, Calgary, Canada, Jul. 2009, pp. 1-3.
[34] G. Johnson and I. Beausoleil-Morrison, "Electrical-end-use data from 23 houses sampled each minute for simulating micro-generation systems," *Applied Thermal Engineering*, vol. 114, pp. 1449-1456, Mar. 2017.
[35] S. Ramos, J. Soares, T. Pinto *et al*. (2013, Feb.). Short-term wind forecasting to support virtual power player operation. [Online]. Available: http://hdl.handle.net/10400.22/58902013.
[36] Green Cars Compare. (2023, Jan.). Tesla model 3 mid range specs, price, photos, offers and incentives. [Online]. Available: https://evcompare.io/cars/tesla/tesla-model-3-midrange-rwd/.
[37] J. Antoun, M. E. Kabir, B. Moussa *et al*., "Impact analysis of level 2 EV chargers on residential power distribution grids," in *Proceedings of 2020 IEEE 14th International Conference on Compatibility, Power Electronics and Power Engineering* (*CPE-POWERENG*), Setubal, Portugal, Jul. 2020, pp. 523-529.
[38] *IEEE Standard for Interconnection and Interoperability of Distributed Energy Resources with Associated Electric Power Systems Interfaces*, IEEE Standard 1547-2018, 2018.

Abdullah Azhar Al-Obaidi received the B.Sc. and the M.Sc. degrees (with honors) in electrical engineering from Khalifa University, Abu Dhabi, United Arab Emirates, in 2011 and 2013, respectively, and the Ph.D. degree in electrical engineering and computer science from York University, Toronto, Canada, in 2022. He is a recipient of several awards, including the Mitacs Accelerate and the Ontario Government Scholarships in Canada. He has over three years of industrial experience in commissioning and maintenance of islanded microgrid systems. His current research interests include electric vehicles, integrated hydrogen and power systems as well as transactive energy.

Mohamed Zaki El-Sharafy received the B.Sc. (with honors) and the M.Sc. degrees in electrical engineering from Arab Academy for Science, Technology, and Maritime Transport, Cairo, Egypt, in 2010 and 2014, respectively, and the Ph.D. degree in electrical and computer engineering from York University, Toronto, Canada, in 2019. Since September 2022, he has been with the Department of Engineering Studies in the Independent Electricity System Operator (IESO), Mississauga, Canada, where he is currently working

as an Power System Analyst. He is also working as a Part-time Professor with Seneca College and Humber College, Toronto, Canada, teaching electrical courses related to power system dynamics and power electronic systems. His current research interests include smart grids, islanded microgrids, electric vehicles, storage systems, integrated power and natural gas system, and application of blockchain technology for smart grid.

Hany E. Z. Farag received the B. Sc. (with hons.) and M. Sc. degrees in electrical engineering from Assiut University, Assiut, Egypt, in 2004 and 2007, respectively, and the Ph.D. degree in electrical and computer engineering from the University of Waterloo, Waterloo, Canada, in 2013. Since July 2013, he has been with the Department of Electrical Engineering and Computer Science, Lassonde School of Engineering, York University, Toronto, Canada, where he is currently an Associate Professor and York Research Chair in Integrated Smart Energy Grids. He is a Registered Professional Engineer in Ontario and a recipient of the Early Researcher Award (ERA) from the government of Ontario. He is the Principal Investigator of over $3M projects funded from NSERC, Ontario Goverment, MITACS, and several industry partners such as the IESO, Alectra Inc., EDA, TROES Inc., CUTRIC, and Hydrogenics. His current research interests include integration of distributed and renewable energy resources, transportation electrification, green hydrogen generation and storage, modeling, analysis, and design of microgrids, and applications of multi-agent, and blockchain technologies in smart grids.

Saifullah Shafiq received the B. Sc. degree in electrical engineering from the University of Engineering & Technology, Lahore, Pakistan, in 2014, and the M.Sc. degree in electrical engineering from the King Fahd University of Petroleum & Minerals, Dhahran, Saudi Arabia, in 2017. He is currently working toward the Ph. D. degree with Electrical Engineering Department, University of Queensland (UQ), Brisbane, Australia. Before joining UQ, he was a Lecturer with Prince Mohammad Bin Fahd University (PMU), Al-Khobar, Saudi Arabia. His current research interests include power system planning, renewable energy resources, electric vehicles, and demand-side management.

Ali Al-Awami received the Ph. D. degree in electrical engineering from the University of Washington, Seattle, USA, in 2010. He is currently an Associate Professor with the Department of Electrical Engineering, and a Research Affiliate with the Inter-disciplinary Research Center for Smart Mobility and Logistics, King Fahd University of Petroleum & Minerals, Dhahran, Saudi Arabia. His industrial experiences include working for the Saudi Electricity Company, Saudi Aramco, and Bonneville Power Administration. He is a Member of the IEEE Water-Power Systems Task Force and IEEE Global Circuit Catalogue Task Force. His research interests include optimization, operation, and control of integrated/hybrid energy systems, integration of distributed energy resources into the smart grid, and electrified mobility.